Journal of Heredity, 2025, **116**, 101–112
https://doi.org/10.1093/jhered/esae034
Advance access publication 1 July 2024
Original Article

Original Article

Mutation of *mpv17* results in loss of iridophores due to mitochondrial dysfunction in tilapia

Jia Xu[1,†], Peng Li[1,†], Mengmeng Xu[1], Chenxu Wang[1,*], Thomas D. Kocher[2] and Deshou Wang[1,*]

[1]Integrative Science Center of Germplasm Creation in Western China (CHONGQING) Science City, Key Laboratory of Freshwater Fish Reproduction and Development (Ministry of Education), Key Laboratory of Aquatic Science of Chongqing, School of Life Sciences, Southwest University, Chongqing 400715, China,
[2]Department of Biology, University of Maryland College Park, Maryland, United States

[†]These authors contributed equally to this work.
[*]Corresponding authors: Email: wdeshou@swu.edu.cn (DW); wolfgang0625@163.com (CW)

Corresponding Editor: Elaine Ostrander

Abstract

Mpv17 (mitochondrial inner membrane protein MPV17) deficiency causes severe mitochondrial DNA depletion syndrome in mammals and loss of pigmentation of iridophores and a significant decrease of melanophores in zebrafish. The reasons for this are still unclear. In this study, we established an *mpv17* homozygous mutant line in Nile tilapia. The developing mutants are transparent due to the loss of iridophores and aggregation of pigment granules in the melanophores and disappearance of the vertical pigment bars on the side of the fish. Transcriptome analysis using the skin of fish at 30 dpf (days post fertilization) revealed that the genes related to purine (especially *pnp4a*) and melanin synthesis were significantly downregulated. However, administration of guanine diets failed to rescue the phenotype of the mutants. In addition, no obvious apoptosis signals were observed in the iris of the mutants by TUNEL staining. Significant downregulation of genes related to iridophore differentiation was detected by qPCR. Insufficient ATP, as revealed by ATP assay, α-MSH treatment, and *adcy5* mutational analysis, might account for the defects of melanophores in *mpv17* mutants. Several tissues displayed less mtDNA and decreased ATP levels. Taken together, these results indicated that mutation of *mpv17* led to mitochondrial dTMP deficiency, followed by impaired mtDNA content and mitochondrial function, which in turn, led to loss of iridophores and a transparent body color in tilapia.

Key words: iridophore, melanophore, mitochondrial dysfunction, *mpv17* mutation, tilapia

Introduction

The *mpv17* gene encodes a highly conserved mitochondrial inner membrane protein (Spinazzola et al. 2006). The exact function of Mpv17 is still unclear, even though most studies suggest that it acts as a transport channel similar to PXMP2 (Antonenkov et al. 2015; Mukherjee et al. 2023). Electrophysiological observation reveals that MPV17 recombinant protein forms a nonselective channel with a pore size of about 1.8 nm, which is sufficient for almost all mitochondrial solutes to pass through (Spinazzola et al. 2006). Knockdown of *MPV17* in HeLa cells results in disruption of folate-mediated one-carbon metabolism and incorporation of uracil into mtDNA (mitochondrial DNA). These results suggest that MPV17 might be a channel for transporting dTMP-associated nucleotides because the presence of uracil in mtDNA is a marker of folate disorders and impaired dTMP (deoxythymidine monophosphate) synthesis (Alonzo et al. 2018). Furthermore, *Mpv17* ablation in mice leads to a significant reduction in dTTP (deoxythymidine triphosphate) and a severe decrease of dGTP (deoxyguanosine triphosphate)) (Dalla Rosa et al. 2016). These results suggest that Mpv17 is a nucleotide-related transport channel, especially for dTMP, in mitochondria in mammals.

Mpv17 deficiency causes severe mitochondrial DNA depletion syndrome (MDDS) in mammals, a class of mitochondrial diseases characterized by varying degrees of reduction in mtDNA content (Löllgen and Weiher 2015). The number of mitochondria and the content of mtDNA in different tissues is variable, which causes obvious phenotypic differences after *MPV17* mutation, especially in tissues with high mitochondrial activity such as the liver, muscles, and nervous system, where mitochondrial activity is often severely affected (Karadimas et al. 2006). Interestingly, the different mutants of *mpv17* in zebrafish show different phenotypes. The CRISPR/Cas9-knockout mutants exhibit no significant changes in mtDNA copy number in whole zebrafish. The natural *mpv17* mutants *tra* exhibit little difference in mtDNA content in liver, muscle, and brain tissues (Krauss et al. 2013; Bian et al. 2021), while natural *mpv17* mutants (e.g. *roy*) show significantly reduced mtDNA contents in embryos at 10 dpf and in

Received March 19, 2024; Accepted June 15, 2024

the skin tissue of adult fish (D'Agati et al. 2017; Martorano et al. 2019). mtDNA is essential for the normal function of mitochondria. The disordered mtDNA content would impair the energy metabolism as mtDNA encodes some members of the oxidative phosphorylation system (Boore 1999; Suomalainen and Isohanni 2010). In addition, mitochondria are also involved in cholesterol and steroid hormone synthesis, β-oxidation of fatty acid, and apoptosis (Bratic and Trifunovic 2010; El-Hattab and Scaglia 2016; Basel 2020). Therefore, MDDS associated with *Mpv17* dysfunction in humans and mice is fatal during their early developmental stages (Weiher et al. 1990; El-Hattab et al. 2010). Similarly, the zebrafish *mpv17*-knockout mutants almost all die in 1 month (Krauss et al. 2013; D'Agati et al. 2017; Bian et al. 2021). In contrast, both *tra* and *roy* mutants survive normally and are fertile. Therefore, it is necessary to verify whether *mpv17* mutation affects the mtDNA content and whether the *mpv17* mutants are lethal or viable in other teleosts.

In zebrafish, *mpv17* mutation also causes loss of pigmentation of iridophores and a serious decrease of melanophores during development (Krauss et al. 2013; D'Agati et al. 2017; Bian et al. 2021). Iridophores are pigment cells of neural crest origin that contain orderly stacked guanine crystals forming reflective plates that refract or reflect light and produce a series of structural colors from white to violet (Denton and Land 1971; Fujii 2000; Le Douarin and Dupin 2003; Schartl et al. 2016). Many genes related to iridophores development have been identified, including *tfec*, *pnp4a*, *ednrb1a, ltk*, *sox10*, and the roles of these genes in differentiation, development, and pigmentation of iridophore are relatively clear (Parichy et al. 2000; Dutton et al. 2001; Kimura et al. 2017; Petratou et al. 2018). The *mpv17* and *mitfa* double mutation results in *casper*, a complete transparent zebrafish strain, but the reason for the defects in iridophores and melanophores after *mpv17* mutation is still unknown (Krauss et al. 2013; D'Agati et al. 2017). In addition, there has been no study examining the global gene expression profile after mutation of *mpv17*. As tetrapods do not have iridophores, mutation of *mpv17* in teleosts provide a new direction to further understand the function of Mpv17.

In zebrafish, iridophores normally appear early in the development of wild-type fish, but in *tra* and *roy* mutants they almost completely disappear in later developmental stages. The purinosome in the residual iridophores in the mutants at 5 dpf (days post fertilization) exhibit a high degree of vesiculation similar to autophagosomes, indicating apoptosis of iridophores after differentiation (Krauss et al. 2013). In *mpv17* knockout mutants, the iridophores are significantly reduced during early development, but can be restored by remedying dNTP (deoxynucleotide triphosphate) and orotic acid (Martorano et al. 2019). In addition to the loss of iridophores, the *tra* and *roy* mutants also display a decrease in melanophores (Krauss et al. 2013; D'Agati et al. 2017). The iridophores and melanophores in teleosts share a common precursor derived from the neural crest in which *mpv17* is also expressed (Fujii 2000; D'Agati et al. 2017). Therefore, whether the defects of *mpv17* mutants are due to the apoptosis of iridophores, the defects of iridophore pigmentation, or abnormal differentiation of common precursors of melanophores and iridophores remains to be answered. In addition, the normal function of mitochondria is essential to guanine synthesis (Fox and Stover 2008; Ng et al. 2009; French et al. 2016; Steele et al. 2020). Whether the iridophore defects caused by *mpv17* mutation are related to guanine synthesis and mitochondrial dysfunction also remains to be investigated.

In this study, we used CRISPR/Cas9 gene editing to mutate *mpv17* in Nile tilapia and obtained a transparent fish line. We analyzed the phenotype and performed transcriptome analysis using skin samples of fish at 30 dpf. We further administered guanine diets and performed TUNEL staining, qPCR, ATP and melanin assays, α-MSH (melanocyte-stimulating hormone) treatment and *adcy5* mutation analysis, and quantification of mtDNA content to understand the mechanisms underlying the loss of iridophore pigmentation and the loss of melanophore pigmentation. Our results indicate that mutation of *mpv17* leads to impaired mtDNA content and mitochondrial function, which in turn, leads to loss of iridophores and a transparent body color in tilapia.

Materials and methods

The Nile tilapia (*Oreochromis niloticus*) used in this experiment was obtained from the Key Laboratory of Freshwater Fish Resources and Reproductive Development of the Ministry of Education of Southwest University (Chongqing, China). All experimental fishes were cultured in a 26 °C circulating water system under natural light conditions. Offspring were obtained by artificial fertilization and the fertilized eggs were incubated in an artificial incubator with circulating water at 26 °C to obtain the fry. Animal experiments were carried out in strict accordance with the provisions of the guide for the raising and using of laboratory animals, and were approved by the Experimental Animal Ethics Committee of Southwest University.

Mutation of *mpv17* and establishment of homozygotes

The target sequence (GGCCTTGGAGAGGCTACCAGG) was selected from the second exon of the tilapia *mpv17* by the online website (http://crispr.dbcls.jp/), using an AGG PAM region. The Cas9-mRNA and guide-RNA were synthesized as reported previously (Li et al. 2014). Cas9-mRNA (1000 ng/μL) and guide-RNA (500 ng/μL) were mixed evenly at a ratio of 1:1, and a 1/10 volume of phenol red was added as an indicator before microinjection of the mixture into zygotes. F0 chimera mutants were verified by restriction enzyme digestion with *Bst*N I. F1 heterozygous with different mutation types were obtained by crossing F0 chimeric male fish with wild-type XX female fish and the mutation types were identified by Sanger sequencing. The +214 bp heterozygous mutants were chosen to establish mutant line, as this mutation type accounted for the highest proportion of F1 heterozygotes, resulted in frameshift, and allowed easy mutant screening in agarose gel. The primers used for gRNA (guide RNA) synthesis were as follows:

mpv17-gRNA-F: TAATACGACTCACTATAGGCCTTTG GAGAGGCTACCGTTTTAGAGCTAGAAATAGC and

mpv17-gRNA-R: AGCACCGACTCGGTGCCAC

qPCR (quantitative polymerase chain reaction)

Total RNA from tilapia tissues of adult (n = 3) and 5 dpf whole embryos (n = 20) was extracted by RNAiso (Takara, Japan) and the RNA concentration was determined by Nanodrop 2000 (Thermo, USA). Primescript RT reagent kit with gDNA eraser (Takara, Japan) was used for reverse transcription and cDNA (complementary DNA) synthesis, which was diluted 10-fold as a template for real-time quantitative PCR (polymerase chain

reaction). Real-time quantitative PCR was performed using TB Green Premix Ex Taq II (Takara, Japan) and the relative expression levels were calculated using the formula $R = 2^{-\Delta\Delta Ct}$. β-*actin* was used as an internal reference gene. Specific gene primers can be found in Supplementary Table 1.

Phenotype analysis and chromatophore counting

Five wild-type fish and 5 *mpv17*$^{-/-}$ mutants were photographed at 3, 5, 30, and 90 dpf. Fish less than 30 dpf were photographed using Leica M165FC stereomicroscope (Leica, Germany), while fish at 90 dpf were photographed using Nikon D7000 camera (Nikon, Japan). The shape and number of melanophores in the skin vertical bars, non-barred areas, dorsal fins, tail fins, and anal fins of 90 dpf mutants were quantified by taking photos and counting. To facilitate the counting of skin chromatophores, fishes were anesthetized with 4.5 mg/mL Tricaine (MS-222, USA) and then placed in a 10 mg/mL L-Adrenaline (Sigma, USA) solution for 15 min to contract the chromatophores. Surgical scissors were used to cut off 25 mm^2 sized fin pieces which were placed on a glass slide and photographed using an Olympus optical microscope BX53 (Olympus, Japan). Differences in the number of chromatophores were analyzed using GraphPad Prism 8.01 software (GraphPad, USA).

Transcriptome analysis

The skin tissue of wild-type and *mpv17* mutant fish ($n = 3$) at 30 dpf were removed to extract the total RNA. The integrity and quantity of total RNA was characterized by specialized agarose electrophoresis, and the purity was measured using the Nanodrop2000. The mRNA was then fragmented to 300 bp using a solution of Mg^{2+}. The first strand of cDNA was synthesized by reverse transcription using 6-base random primers, and the second strand cDNA was synthesized using the first strand cDNA as a template. The sequencing library was enriched by amplifying cDNA with high-fidelity polymerase. The size of the library was quantified using an Agilent 2100 Bioanalyzer (Agilent Technologies, USA) and the total concentration of the library was quantified by real-time PCR. Transcriptome sequencing was performed on the Illumina HiSeq 2000 RNA-Seq platform (Illumina, USA). A single-stranded library was prepared from 0.75 μg of RNA and then used as a template for bridge PCR amplification. Then the raw data was filtered to remove low-quality reads, adaptor reads, and ambiguous nucleotides. The clean reads were aligned to the reference genome of tilapia (GCF_001858045.2_O_niloticus_UMD_NMBU_genomic.fna) by using HISAT2 software (Kim et al. 2019). The expression level of each gene was calculated and used for expression difference analysis, enrichment analysis, and cluster analysis. The reads were assembled to restore the transcript sequence.

Guanine treatment

The wild-type fish and *mpv17*$^{-/-}$ mutants ($n = 20$) at 60 dpf were fed with 6 mg/g guanine-treated diets three times a day for 5 weeks. The phenotypes were recorded using a Leica stereo microscope (Leica, Germany). The liver tissues of the control and treated fish ($n = 3$) were sampled to extract RNA for detection of *gda* (a key gene involved in guanine catabolism and highly expressed in the liver) expression to verify the intake of guanine at the end of the treatment.

TUNEL apoptosis assay

Wild-type and mpv17$^{-/-}$ mutants of 5 dpf ($n = 6$) were fixed with 4% PFA (phosphonoformate) overnight at 4 °C. The fixed materials were washed with PBS and then processed by gradient ethanol dehydration, xylene transparency, and paraffin embedding. The embedded materials were sliced and pasted onto glass slides. Then xylene, gradient ethanol, and 0.3% Triton X-100 were used to dewa, rehydrate, and penetrate, respectively. After washing in PBS, TUNEL testing solution was prepared according to the One Step TUNEL Apoptosis Assay Kit (Beyotime, China) and incubated in the dark at 37 °C for 1 h. The slides were washed in PBS again and sealed; finally, photos were taken with an Olympus FV3000 laser confocal microscopy (Olympus, Japan).

α-MSH treatment

Wild-type fish and mpv17$^{-/-}$ mutants ($n = 3$) at 30 dpf were put into a solution of 1 mM α-MSH for 30 min to disperse the melanosomes. Photos of the body and the melanophores of vertical bars were taken before and after treatment using a stereomicroscope (Leica, Germany).

Melanin content quantification

The eyes, peritoneum, and skin tissues of wild-type and mpv17$^{-/-}$ mutants ($n = 4$) at 30 dpf were removed and cleaned with PBS. Then these tissues were dried in an oven. About 10 mg of each dried sample were dissolved in 1M NaOH for 4 h at 85 °C. A Multiskan Go (Thermo, USA) microplate reader was used to measure the absorbance at 375 nm. Each sample was tested three times with 1M NaOH used as a blank. The relative melanin content was calculated by dividing the absorbance of each sample by the average absorbance of wild-type fish.

ATP content quantification

ATP (adenosine triphosphate) content was quantified using the ATP Assay Kit (Beyotime, China). The ATP standard solution was diluted with lysis buffer to seven concentrations: 10, 30, 100, 300, 1,000, 3,000, and 10,000 nM. The chemiluminescence was detected with Luminoskan Ascent (Thermo, USA) to obtain a standard curve. Fish at 5 dpf ($n = 20$) and skin (20 mg) from fish at 30 dpf ($n = 5$) were homogenized with 200 μL lysis solution. After centrifugation at 12,000 *g* for 5 min at 4 °C, the supernatant was collected, and the protein concentration was measured by the Nanodrop2000 (Thermo, USA). The ATP detection solution was added to the supernatant. The actual value of chemiluminescence was detected. The luminescence value was divided by the protein concentration to convert ATP concentration into nmol/g protein value for eliminating interference of protein concentration differences. The average value of wild-type was used as the standard. The relative ATP content was calculated by dividing the mutant value to the average value of the wild-type.

mtDNA content detection

The *nd1* (mitochondrial gene) and *enc1* (nuclear gene) gene fragments were amplified by PCR using genomic DNA extracted from tilapia fins with gene-specific qPCR primers, the primers were listed in Supplementary Table 1. The PCR

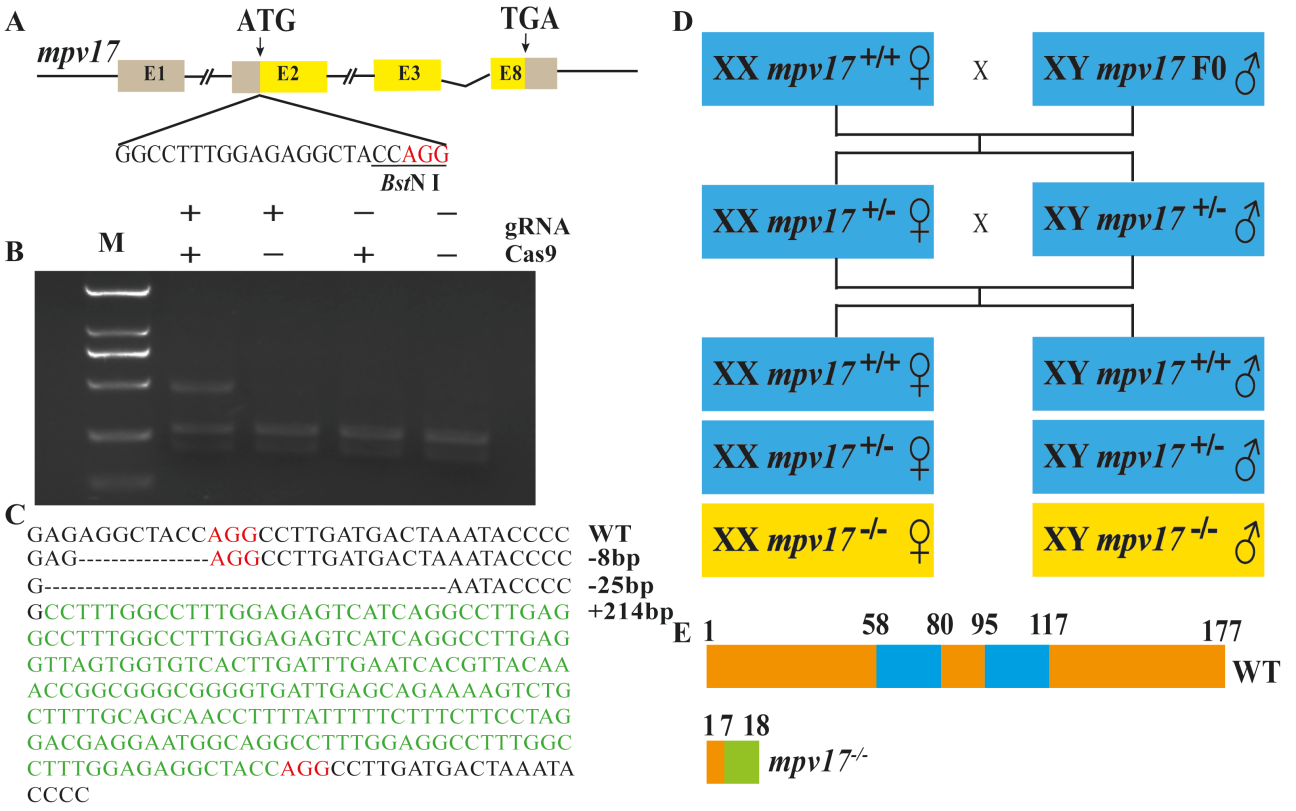

Fig. 1. Target selection and establishment of tilapia *mpv17* homozygous mutant line. Gene structure of *mpv17* in tilapia showing target sequences and PAM region on exon 2, with a restriction endonuclease *Bst*N I cleavage site on this target (A). The mutation was confirmed by restriction enzyme digestion, the unmutated DNA from the embryos injected with either Cas9-mRNA or *mpv17*-guide-RNA was cleaved into two bands, while mutated DNA from the embryos injected with Cas9-mRNA and *mpv17*-guide-RNA showed an uncleaved band (B). Mutant types of F1 offspring produced by F0 XY male fish and wild-type XX female fish were identified by Sanger sequencing, and the type of +214 bp was selected to establish the homozygous mutant line, the added nucleotide sequence was indicated in green (C). The process of establishing the homozygous mutant line (D). The normal and mutated protein structures of Mpv17 of tilapia, the blue box represented the domain of transmembrane region. The mutation of +214 bp caused a frameshift and a premature stop codon, which resulted in only 18 amino acids in the peptide and only 6 amino acids were consistent with those in the wild-type (E). M, DNA Marker DL2000. WT, wild-type.

products were purified, cloned into the pMD19-T vector (Takara, Japan), and transformed into DH5α (Tsingke, China). The plasmids were extracted and linearized with *Sac*I to obtain the standard plasmid. The concentration of standard plasmid was converted into copy number using the formula copy/μL = (6.02 × 1023 × *n*)/(660 × *m*), where "*n*" represents concentration and "*m*" represents numbers of base pairs. The standard plasmid was serially diluted by 10-fold. qPCR was performed to obtain CT values in different copy numbers to draw standard curves. Subsequently, qPCR was performed using genomic DNA extracted from fish (both wild-type and mutants) at 5 dpf and skin from fish (both wild-type and mutants) at 30 dpf to obtain CT values and compared to the standard curves to determine the corresponding copy numbers. The mtDNA content was calculated by the following formula: mtDNA content = (2 × mtDNA copy number)/nDNA copy number. Finally, the relative mtDNA content was obtained by dividing the mtDNA content of mpv17$^{-/-}$ mutants to the average of that of wild-type.

Data analyses

All data were expressed as mean ± SD and Student's *t*-test was used to determine the differences between the two groups. The data were statistically analyzed using the GraphPad Prism 8.01 software (GraphPad, USA). In all analyses, "*" represented statistical difference ($P < 0.05$), "**" represented significant difference ($P < 0.01$), "***" represented extremely significant difference ($P < 0.001$), and "ns" represented no significant difference.

Results

Establishment of tilapia *mpv17* homozygous mutants

A specific target (GGCCTTGGAGAGGCTCCAGG) was designed in the second exon of the *mpv17* gene of Nile tilapia. CRISPR/Cas9 gene editing was used to knockout this gene (Fig. 1A). Wild-type XY zygotes were microinjected with *mpv17*-guide-RNA and Cas9-mRNA mix to obtain F0 chimeras. The target sequence was digested with *Bst*N I to verify whether the mutation was successful. An undigested band was observed when the *mpv17*-guide-RNA and Cas9-mRNA were injected simultaneously and mutated the site successfully (Fig. 1B). After the F0 generation chimeras were sexually mature, they were mated with wild-type XX female fish to obtain the F1 heterozygotes. Various types of F1 heterozygotes were identified by Sanger sequencing (Fig. 1C). The +214 bp heterozygous mutants were chosen to

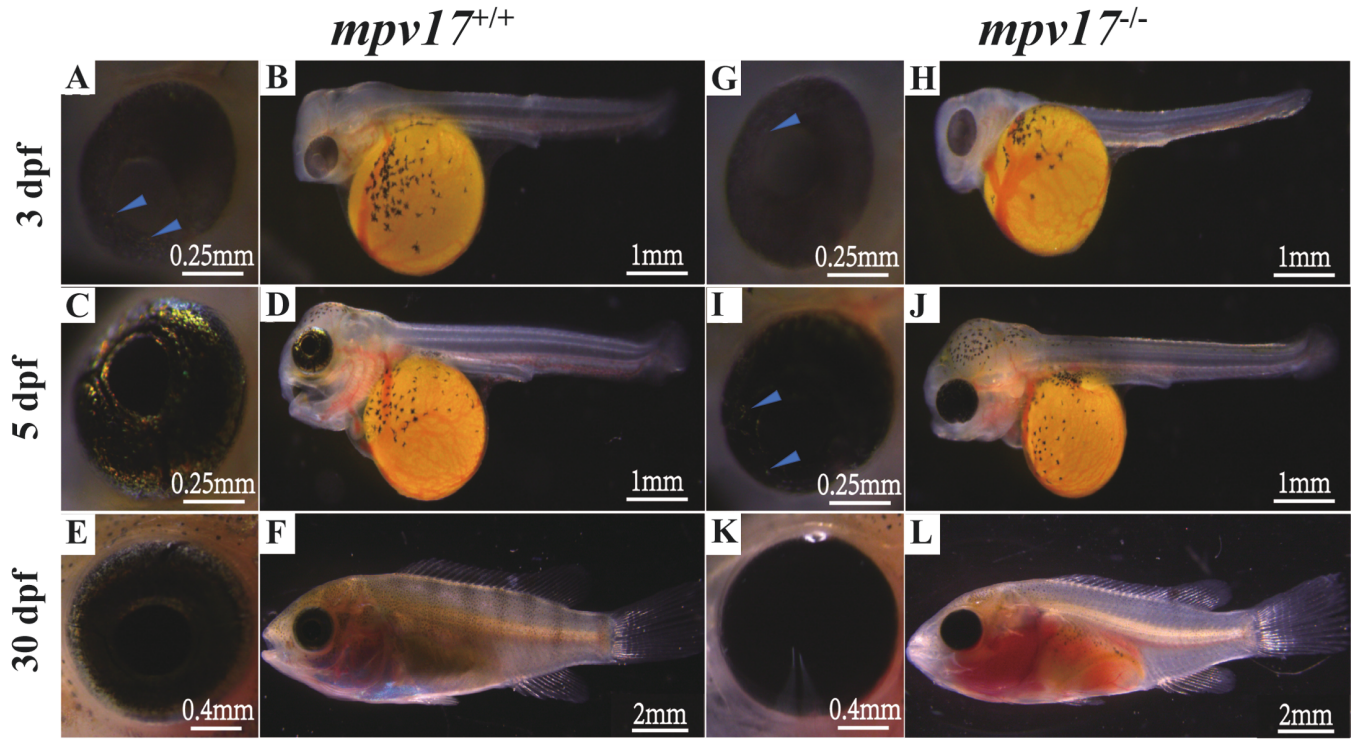

Fig. 2. The *mpv17* mutants displayed transparent phenotype with few iridophores at larval and juvenile stage in tilapia. At 3 dpf, some iridophores were observed on the iris in wild-type fish (A, B), while few iridophores were observed in *mpv17*$^{-/-}$ mutants (G, H). At 5 dpf, increased iridophores was observed on the iris in wild-type fish (C, D), while almost no iridophores were observed in *mpv17*$^{-/-}$ mutants (I, J). At 30 dpf, the whole body of wild-type fish was almost covered up by iridophores, with melanophore-pigmented black vertical bars on the trunk (E, F). In contrast, in *mpv17*$^{-/-}$ mutants, no iridophores and no black bars (but with some melanophores visible), were observed, displaying a transparent phenotype (K, L). dpf, days post fertilization.

establish mutant line, as this frameshift mutation accounted for the highest proportion of F1 heterozygotes and allowed easy mutant screening in agarose gel. An F2 generation was obtained by mating +214 bp F1 male with the same mutation type female. F2 fishes were screened for homozygous *mpv17* mutants (Fig. 1D). This mutation causes the frameshift mutation and premature termination of Mpv17 translation (Fig. 1E).

Mutation of *mpv17* led to a transparent body color in tilapia

Iridophores began to appear on the iris in wild-type fish at 3 dpf (Fig. 2A and B), significantly increased on the iris at 5 dpf (Fig. 2C and D), also appeared on the peritoneum at this time (Supplementary Fig. S1), and gradually covered the body surface at 30 dpf (Fig. 2E and F). In *mpv17*$^{-/-}$ mutants, a few iridophores appeared at 3 dpf (Fig. 2G). Except for this, these were no obvious differences between the wild-type and mutants during this period (Fig. 2B and H). The iridophores of mutants stopped increasing (Fig. 2I and J), and finally disappeared during later development (Fig. 2K and L). In addition, the wild-type fishes displayed clear black vertical bars at 30 dpf (Fig. 2F). In contrast, no vertical bars were observed in the mutants at this time (Fig. 2L). The absence of iridophore pigmentation and black bars led to a transparent body color in the mutants, with the viscera clearly visible (Fig. 2L). At 90 dpf, iridophores covered the whole trunk surface of the wild-type fish (Fig. 3A). Two types of melanophores, dendritic, and punctate melanophores, were observed to form the bars and inter-bars, respectively (Fig. 3B). The *mpv17*$^{-/-}$ mutants displayed the color of muscle with the black peritoneum visible (Fig. 3F). Statistically, no significant differences in melanophore number were observed on the body surface between the wild-type and mutants (Fig. 3G and K). Most of the dendritic melanophores became punctate and failed to form bars in *mpv17*$^{-/-}$ mutants (Fig. 3G). Interestingly, the melanophores in the fins were normal, both in number and shape (Fig. 3L).

Transcriptome analysis of skin tissue in *mpv17* mutants and wild-type fish

Transcriptome sequencing was performed using skin tissues from *mpv17*$^{-/-}$ mutants and wild-type fish ($n = 3$) at 30 dpf. A total of 26,909 genes were annotated according to the sequencing results, covering over 95% of the tilapia genome. Among them, 492 genes were significantly upregulated, 778 genes were significantly downregulated, and 25,639 genes were not significantly changed in *mpv17*$^{-/-}$ mutants compared with wild-type (Fig. 4A). The clustering of our samples is shown in the heatmap (Fig. 4B). KEGG (kyoto encyclopedia of genes and genomes) enrichment analysis showed that the differentially expressed genes (DEGs) were enriched in five categories, including cellular processes, environmental information processing, human diseases, metabolism, and organismal systems. Among these, the category of metabolism was the most obviously enriched. The one-carbon pool by folate, steroid hormone biosynthesis, and purine metabolism pathways

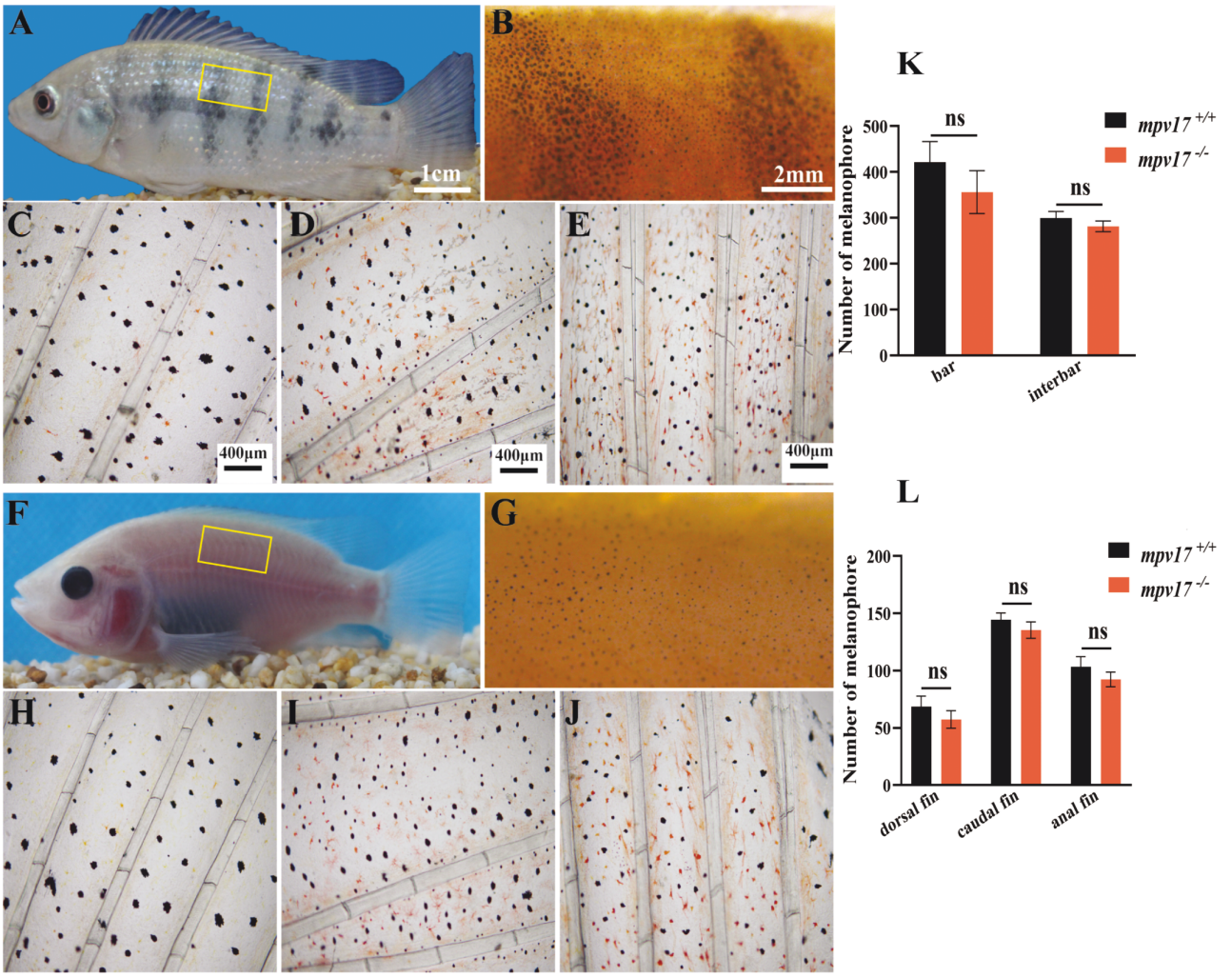

Fig. 3. The mutants displayed pink-colored semi-transparent phenotype with no iridophores and punctuated melanophores at 90 dpf. At 90 dpf, the wild-type fish displayed silver–white body color due to the coverage of iridophores and with 7–9 black vertical bars formed by dendritic melanophores (A, B). In *mpv17*$^{-/-}$ mutants, no iridophore pigmentation and dendritic melanophores, punctuated melanophores (equal number of the dendritic and punctuated melanophores observed in the wild-type fish) were observed (K), displaying a pink-colored semi-transparent phenotype (F, G). No differences were observed between the wild-type fish and *mpv17*$^{-/-}$ mutants in shape of melanophores, xanthophores, and erythrophores in dorsal fin (C, H), caudal fin (D, I), and anal fin (E, J). Statistical analysis revealed no significant changes in number of melanophoresbetween the wild-type fish and *mpv17*$^{-/-}$ mutants (L).

were significantly enriched, and some other pathways such as lipid metabolism and amino acid metabolism were also enriched (Fig. 4C). Most of these metabolic processes occur in or were related to mitochondria, reflecting severe defects in mitochondrial metabolism. Genes related to the de novo synthesis of purine, like *gart*, *pfas*, *paics*, and *atic* which are involved in the processing of PRPP (5-phosphoribosyl 1-pyrophosphate) to IMP (inosinemonphosphate), were significantly downregulated. In addition, genes involved in purine catabolism, including *xdh* and *pnp4a*, were also downregulated (Fig. 4D). The one-carbon pool by folate pathway, with all the enriched genes downregulated, was the most enriched pathway (Fig. 4C and E). Surprisingly, the genes associated with both folate-dependent de novo dTMP synthesis and salvage synthesis in mitochondria were upregulated (Fig. 4F). In addition, expression of genes related to differentiation and survival of melanophores, such as *mitf*, *kita*, *foxd3*, etc., were normal (Fig. 4G), while most genes related to melanin synthesis, such as *dct*, *pmel*, *tyrp1*, etc., were downregulated (Fig. 4H).

Abnormal differentiation of pigment cell precursors led to loss of iridophores

The loss of iridophore pigmentation might have arisen from either guanine insufficiency or loss of iridophores. Thus, we first fed *mpv17*$^{-/-}$ mutants with guanine-containing feed for 5 weeks, but failed to rescue the iridophore pigmentation (Fig. 5A). The expression level of *gda* in guanine-treated fish increased significantly compared with the control group, indicating successful ingestion of guanine (Fig. 5B). These results demonstrated that the phenotype of the mutants was caused by loss of iridophores, either apoptosis or abnormal differentiation of precursors, rather than guanine insufficiency. We further performed TUNEL assays, however, we did not find obvious signals of apoptosis in the iris (Fig. 5C). Apoptosis occurred in some cells of the whole fish, but not the iridophores of iris. Then we examined the expression of genes related to iridophore differentiation, including *sox10*, *tfec*, *ednrba*, *ltk*, and *pnp4a*. All of these genes were significantly downregulated in the mutants compared with the wild-type

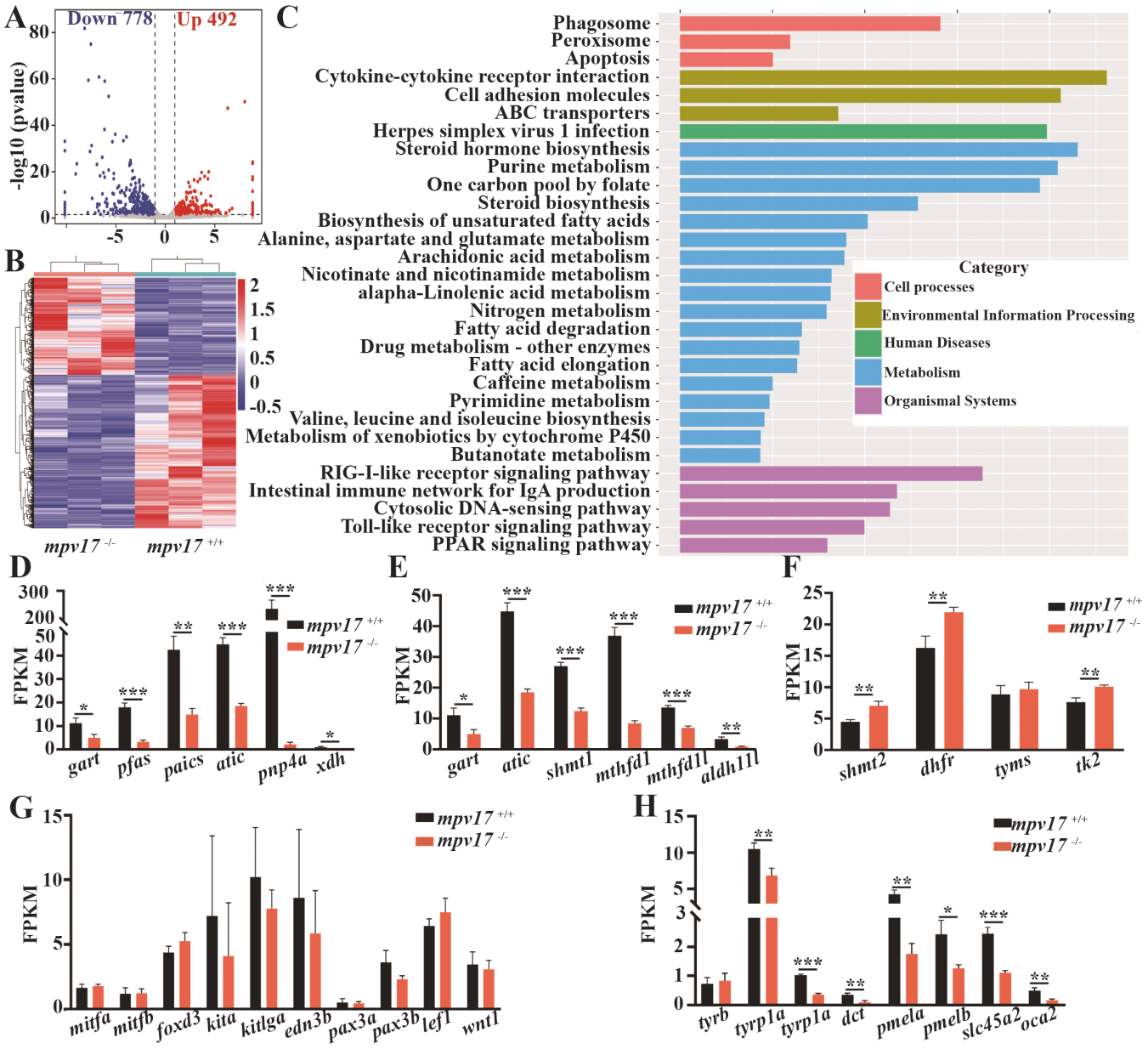

Fig. 4. Transcriptome analysis of differentially expressed genes between skin of mutants and wild-type fish at 30 dpf. A total of 26,909 genes were annotated in the sequencing results, covering more than 95% of the tilapia genome. Among them, 492 genes were upregulated and 778 genes were downregulated (A). Heatmap generated by gene expression clustering between wild-type and *mpv17*$^{-/-}$ mutants (B). KEGG enrichment analysis of differentially expressed genes (DEGs). The top 20 enriched pathways were displayed, and the enrichment factor represented the ratio of the number of DEGs in a specific signaling pathway to the total number of genes; the sizes and color of the dots represented the number of genes and FDR (false discovery rate), respectively (C). The DEGs of purine metabolism pathway (D). FPKM of genes related to one-carbon pool by folate (E), dTMP synthesis in mitochondria (F), differentiation and survival of melanophores (G), and melanin synthesis (H). $n = 3$.

fish at 5 dpf (Fig. 5D), indicating abnormal differentiation of iridophores.

Insufficient ATP caused by decreased mtDNA content in melanophores led to melanophore aggregation of the mutants

The aggregation of melanosomes could be the result of limited dispersion of melanin and/or the insufficient melanin content in melanophores due to ATP insufficiency. To verify the former, both wild-type fish and *mpv17*$^{-/-}$ mutants were treated with 1 mM α-MSH (alpha-melanocyte-stimulating hormone) at 30 dpf for 30 min. Compared to untreated fish (Fig. 6A, A', C and C'), enhanced melanin dispersion was observed in both wild-type fish and mutants as reflected by darker body coloration after treatment (Fig. 6B, B', D and D'). However, the treatment failed to produce bars on the trunk of the mutants (Fig. 6D and D'). These results suggested that the morphological function of melanophores was normal in *mpv17*$^{-/-}$ mutants, but the mutation of *mpv*17 led to limited melanosome dispersion. We also examined the melanin content of melanin-deposited tissues, including skin, eyes, and peritoneum, by NaOH digestion, and found that the NaOH digested solution was clearer in *mpv17*$^{-/-}$ mutants than that of wild-type fish (Fig. 6E). The melanin content in the melanin

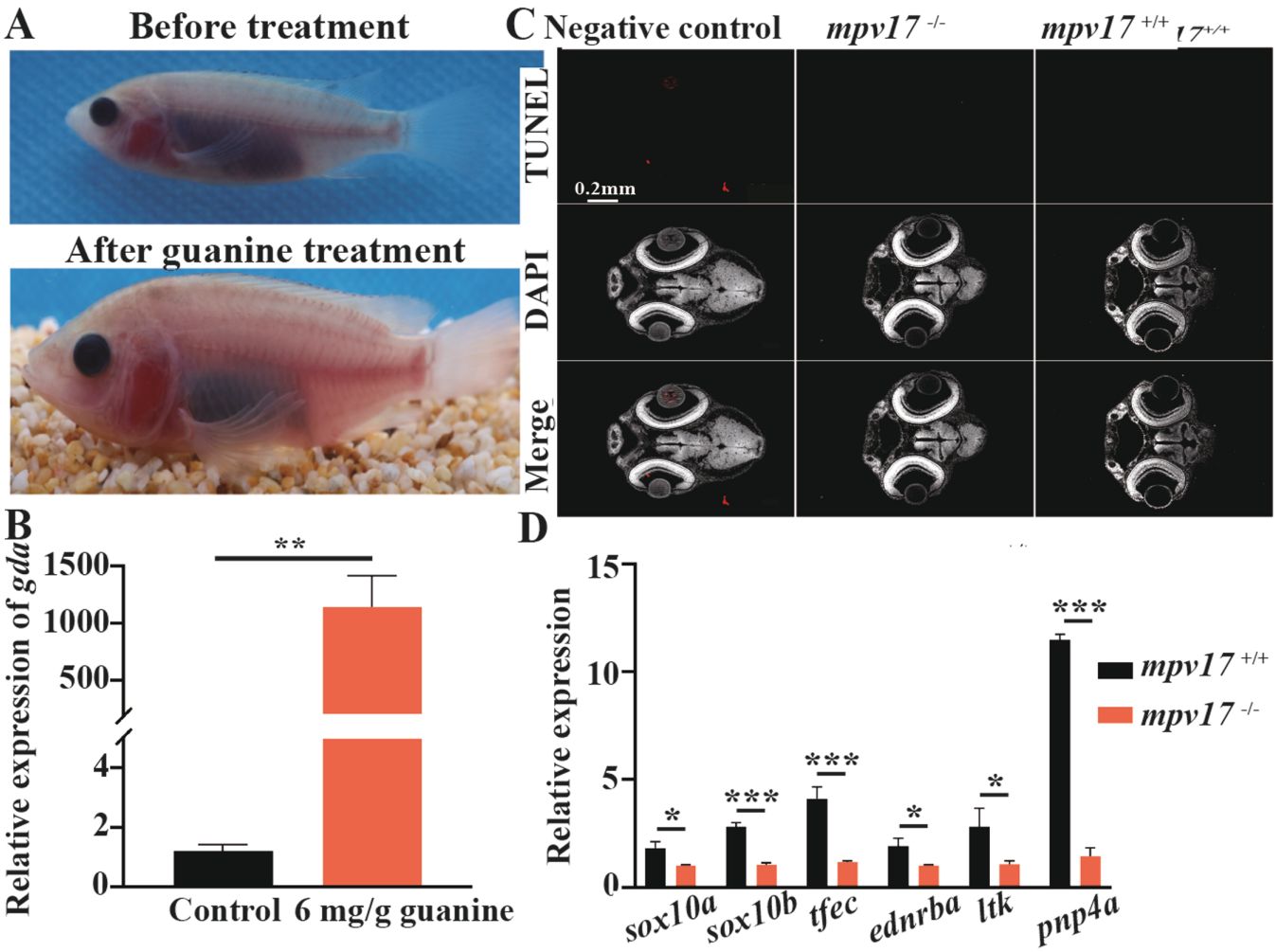

Fig. 5. Abnormal differentiation of iridophore precursor cells in *mpv17* mutants. The *mpv17* mutants at 60 dpf were fed with 6 mg/g guanine-treated diets for 5 weeks, but failed to recover the iridophore pigmentation (A), even though the expression of guanine degradation gene *gda* was significantly upregulated in treatment group (B). No obvious apoptotic signal was observed in mutants and wild-type fish at 5 dpf (C). The expression of genes related to iridophore differentiation was significantly downregulated (D).

deposited tissues was significantly less in the mutants than that in the wild-type fish (Fig. 6F). The ATP content of these tissues in the mutants was less than half that of the wild-type fish (Fig. 6G). Mutation of *adcy5*, the key enzyme for cyclization of ATP into cAMP (cyclic adenosine monophosphate) in melanophores, resulted in loss of bars and increased punctate melanophores in F0 chimeras with high mutant rates (Supplementary Fig. S2). We also detected the mtDNA content of skin at 30 dpf. The mtDNA content in skin of mutants was much less than that in wild-type fish (Fig. 6H). These results suggested that *mpv*17 deficiency resulted in mtDNA deficits leading to low ATP production, indirectly affecting melanin synthesis and diffusion, which in turn, led to an aggregated phenotype in the melanophores. Consistent with that, the mtDNA and ATP content also significantly decreased in the embryos at 5 dpf (Fig. 7A and B).

Discussion

Since the first report of MDDS in humans, the mtDNA depletion caused by *Mpv17* mutation has been confirmed in several organisms, including human, mouse, zebrafish, and yeast (Dallabona et al. 2010; Spinazzola 2011; Krauss et al. 2013; Dalla Rosa et al. 2016; El-Hattab et al. 2017). In this study, we disrupted *mpv17* by CRISPR/Cas9 and investigated the roles of this gene in tilapia. Our results showed that *mpv17* mutation led to a reduction in mtDNA content, mitochondrial dysfunction, loss of iridophores, and aggregation of melanosomes in tilapia.

Studies in zebrafish have shown that the differentiation of neural crest cells into iridophores is progressive, and each process requires corresponding gene expression to promote the differentiation of precursor cells to the next stage, especially *pnp4a* which encodes purine nucleoside phosphorylase that degrades guanosine to guanine. *Pnp4a* is expressed in both iridophores and their precursor cells (Curran et al. 2010; Petratou et al. 2018, 2021). In *tra* mutants, the expression of *pnp4a* is normal in the iridophore precursor cells at the beginning, but sharply downregulated at 48 hpf when no obvious iridophores appear in the wild-type (Krauss et al. 2013). In the present study, a very small number of iridophores and significant downregulation of genes related to iridophore differentiation, including *pnp4a* and *tfec*, was observed in tilapia *mpv17* mutants at 5 dpf. The initial normal expression of *pnp4a* in *tra* mutants and the very small number of iridophores that appeared in tilapia

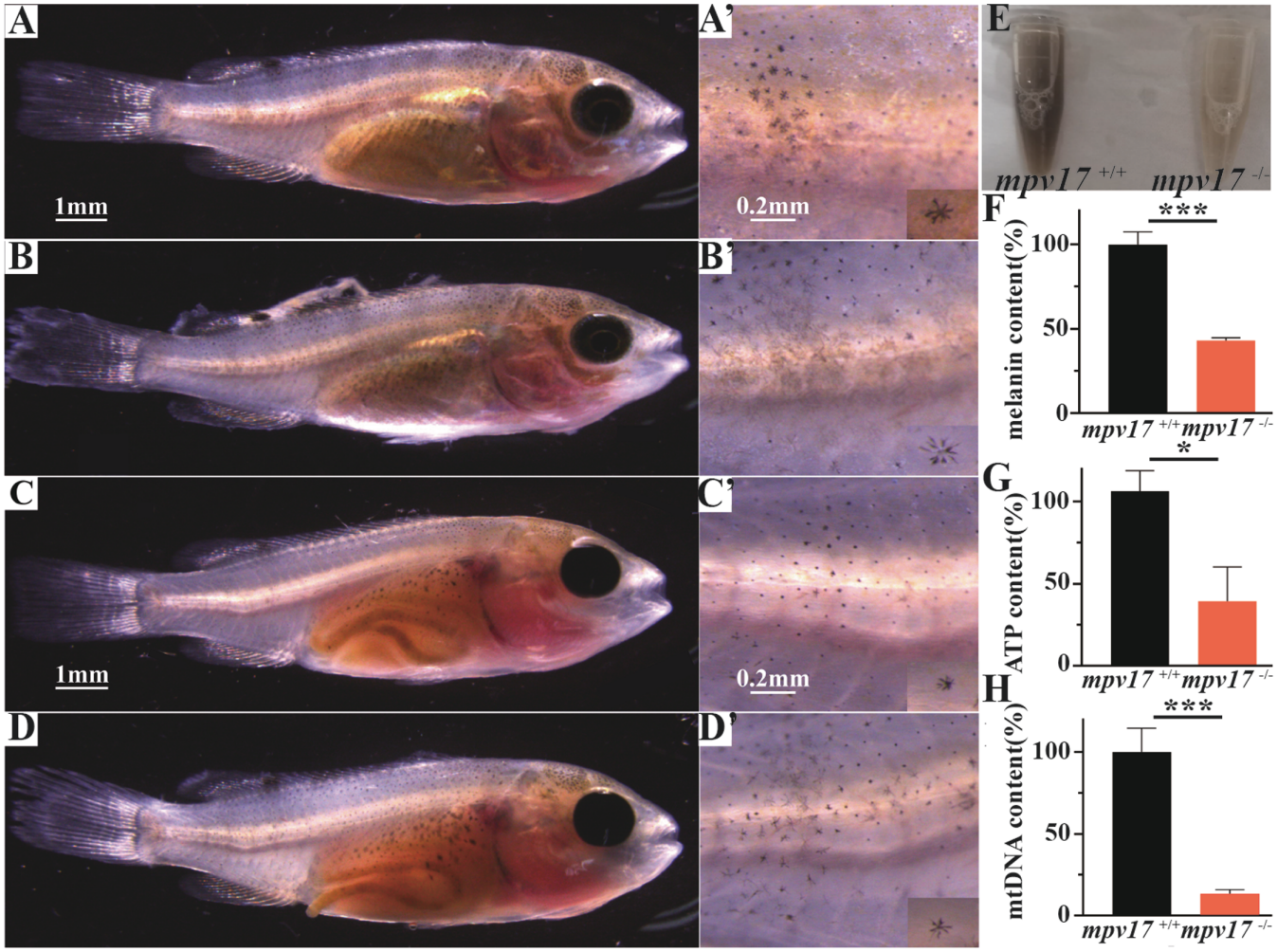

Fig. 6. Limited melanin diffusion and reduced melanin synthesis in *mpv17*$^{-/-}$ mutants. In wild-type fish at 30 dpf, the bars and inter-bars were alternately distributed on the body surface, and the dendritic melanophores exhibited a radiate shape (A, A′). There was no bar-formed color pattern in *mpv17*$^{-/-}$ mutants, the melanophores displayed a limited dispersion and appeared to be punctate at low magnification (B, B′). After treatment with 1 mM α-MSH for 30 min, both the wild-type and *mpv17*$^{-/-}$ mutants became darker (C, C′), and the dendritic melanophores, especially the melanophores in the wild-type, became further dispersed while the punctate melanophores were not affected (D, D′). Compared with wild-type, the NaOH solution of black tissue in *mpv17*$^{-/-}$ mutants was lighter (E), and the melanin content of *mpv17*$^{-/-}$ mutants was less than half than that of the wild-type (F). The ATP contents of skin, eyes, and peritoneum in *mpv17*$^{-/-}$ mutants were even less than a quarter of those of wild-type (G). The mtDNA content of skin in mutants was significantly decreased (H). $n = 3$.

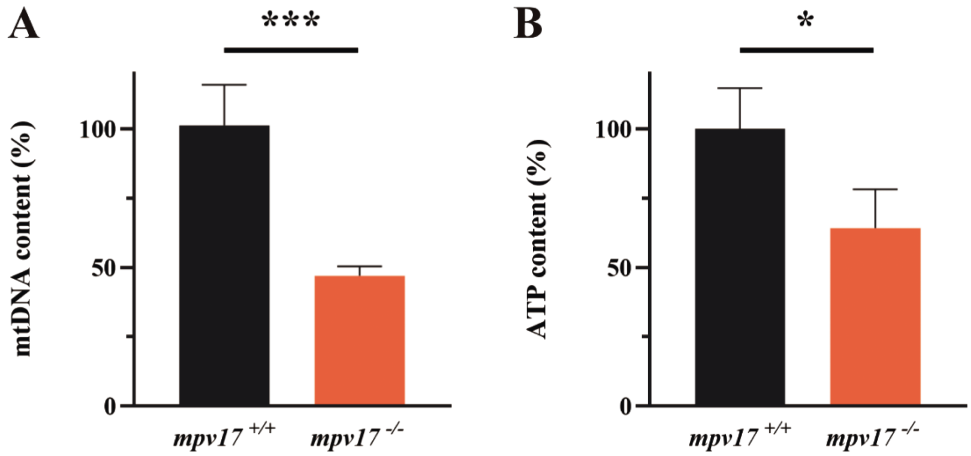

Fig. 7. mtDNA and ATP content in embryos at 5 dpf. The mtDNA and ATP contents were significantly lower in the *mpv17* mutants compared with wild-type fish at 5 dpf (A, B). $n = 20$.

mpv17 mutants might represent the normal function of mitochondria of maternal origin at the early stage (Giles et al. 1980; Artuso et al. 2012). However, as development progresses, the iridophores gradually disappear due to abnormal functions of the newly assembled mitochondria with defects due to Mpv17 deficiency. Another possibility is that there is not enough ATP to support the survival or migration of the iridophore precursor cells. It is well documented that the iridophore precursor cells migrate along specific routes, colonize at a specific location, and differentiate into pigment cells (Kelsh et al. 2009). In this study, guanine diets administration failed to rescue the iridophore pigmentation and no apoptosis of iridophores were observed in the iris of the mutants. Taken together, these results suggest that defects in iridophore differentiation, rather than defects in iridophore pigmentation or apoptosis, are responsible for the loss of iridophores observed in *mpv17* mutants in tilapia. However, there is another possibility that cannot be completely excluded, as purine biosynthesis and normal mitochondrial function have been proved to be inseparable (French et al. 2016; De Vitto et al. 2021). In fact, iridophores were supposed to be alive in the *tra* mutants, but guanine failed to form the structural coloration (Krauss et al. 2013). Therefore, an alternative explanation is that the iridophores were still there, but the guanine crystals could not be formed without normal mitochondrial function in *mpv17* mutants.

The phenotypic differences of melanophores between *mpv17*-mutated zebrafish and tilapia might be related to the differences in color patterning mechanisms. In zebrafish, iridophores were the first chromatophore to appear, and the correct colonization of iridophores specifies the localization of other types of pigment cells. The subsequently appeared melanophores and xanthophores form the horizontal stripes with iridophores (Frohnhöfer et al. 2013; Gur et al. 2020). Therefore, the loss of iridophores also affects other chromatophores and the color pattern. For example, mutation of *bnc2* (basonuclin-2), which is involved in the expansion of the iridophores, leads to loss of iridophores and results in significantly reduced melanophores and xanthophores and almost complete loss of horizontal stripes of the trunk in zebrafish (Lang et al. 2009; Patterson and Parichy 2013). However, in tilapia, melanophores appear first, long before other types of chromatophores, and the formation of vertical bars on its trunk is also dominated by melanophores (Wang et al. 2021; Lu et al. 2022). This explains why a significant decrease in number of melanophores was observed in *mpv17* mutants in zebrafish but not in tilapia. It is well documented that mitochondrial dysfunction impairs energy metabolism and causes insufficient ATP production. ATP could be converted into cAMP which promotes the dispersion of melanosomes and also facilitates melanin synthesis through the cAMP-PKA pathway (Wasmeier et al. 2008; D'Mello et al. 2016). In tilapia *mpv17* mutants, insufficient ATP led to decreased cAMP contents, followed by reduced melanin synthesis and failure of dispersion, which in turn, resulted in miniaturized melanophores and disappearance of vertical bars. In line with this, mutation of *adcy5* in guppy results in the replacement of the corolla and dendritic melanophores observed in wild-type fish with punctate melanophores in the mutants and disappearance of the net-like reticulate pattern which is mainly composed of corolla and dendritic melanophores, in addition, it was also confirmed in zebrafish (Kottler et al. 2015; Zhang et al. 2022a). A similar phenotype of punctate melanophores was observed in tilapia *adcy5* mutants in the present study.

Tilapia *mpv17* mutants are viable and fertile like the zebrafish *tra* and *roy* mutants, different from the low survival rate in *mpv17*-mutated humans, mice, and knockout mutant zebrafish (Weiher et al. 1990; El-Hattab et al. 2010; Krauss et al. 2013; Bian et al. 2021). The normal survival rate in our mutants could be attributed to the Mpv17-like proteins. In zebrafish, the expression of *mpv17l2* (MPV17 mitochondrial inner membrane protein-like 2) was upregulated in *mpv17* null mutant compared to that in the wild-type, and the number of iridophores in mutated larvae increased significantly after *mvp17*-mRNA or *mpv17l2*-mRNA injection, which were supposed to be functional redundancy of Mpv17 and Mpv17-like (Martorano et al. 2019). Consistently, upregulation of *mpv17l2* expression was also observed in our tilapia *mpv17* mutants (Supplementary Fig. S3). However, the *mpv17*-knockout zebrafish die at early developmental stages, and is hard to explain by this view. Interestingly, the knockout zebrafish have seven fewer normal amino acids compared with *tra* mutants, which is suggested to affect the survival of the knockout mutants (Bian et al. 2021). However, our tilapia *mpv17* mutants have even fewer normal amino acids than *tra* and *mpv17* knockout mutants in zebrafish, with a stop codon before the conservative transmembrane structural domain. Therefore, the discrepancy might be attributed to the diversity in tolerance of different animals or different tissues to *mpv17* mutation. For example, in humans, patients with mutation of *MPV17* mainly exhibit the most severely affected liver mtDNA contents and liver diseases; the mouse *Mpv17* mutants often die of nephrotic syndrome and chronic renal failure; while the *mpv17*-knockout zebrafish develop abnormal muscle and liver, thus leading to significant growth restriction (Weiher et al. 1990; El-Hattab et al. 2010; Bian et al. 2021). Consistently, the dysfunction of mitochondria had significant impacts on normal life of tilapia *mpv17* mutants, as demonstrated by delayed growth and spermatogenesis, even though their survival was not affected.

Current research tends to regard Mpv17 as a channel for transporting dNTP in mitochondria (Antonenkov et al. 2015; El-Hattab et al. 2017; Alonzo et al. 2018). It is essential for the balance of the nucleotide pool and the maintenance of the relative abundance of various dNTPs in mitochondria, which is an important prerequisite for supporting normal replication of mtDNA (López et al. 2009; Suomalainen and Isohanni 2010; González-Vioque et al. 2011). Studies of *MPV17* mutated HeLa cells indicate that dTMP is the cargo, as there is an increase in de novo and salvage synthesis of dTMP in mitochondria and a significant incorporation of uracil into mtDNA (Alonzo et al. 2018). In the absence of dTMP mtDNA replication uses uracil, and therefore the incorporation of uracil is a marker of impaired dTMP synthesis (Alonzo et al. 2018; Field et al. 2018). The partial incorporation of uracil into DNA could be recognized and removed by the repair system, but excessive uracil would cause continuous repair and DNA breakage, and even MDDS (Fenech 2001). Consistent with this, mitochondrial thymidine kinase 2 (TK2) deficiency leads to depletion of mitochondrial dTTP pool and causes human MDDS and severe mitochondrial dysfunction (Zhou et al. 2008). In the present study, disordered folate metabolism and dTMP synthesis in skin and decreased mtDNA contents were observed in some tissues. We hypothesized that Mpv17 might be involved in nucleotide

transport for mtDNA synthesis, including deoxy-thymidine and its phosphorylated products (dTMP, dTDP, and dTTP), and even rGMP (riboguanosine monophosphate) as reported in mouse (Moss et al. 2017). Deficiency of Mpv17 leads to a severe shortage of dTMP transported from cytoplasm to mitochondria and increases mitochondria de novo dTMP synthesis for mtDNA synthesis, with serious consumption of the folate, but not enough to compensate the dTMP insufficiency. The imbalanced dNTP and insufficient dTMP result in depletion of mtDNA, leading to subsequent mitochondrial dysfunction, and eventually result in the transparent tilapia.

In summary, these results in the present study indicated that mutation of *mpv17* led to mtDNA contents reduction and mitochondrial dysfunction, which in turn, led to loss of iridophores and a transparent body color in tilapia. The upregulated expression of genes related to dTMP synthesis and the disordered folate pathway in mitochondria imply that the function of Mpv17 was associated with dTMP content. In addition, the disrupted folate pathway provides a possible research direction of the study of iridophores. For example, in GWAS (genome-wide association studies) analysis of some blue and green fighting fish, *mthfd1l*, a key gene for tetrahydrofolate synthesis is found to be a dominant candidate gene (Lee et al. 2017; Zhang et al. 2022b).

Supplementary material

Supplementary material is available at *Journal of Heredity* online.

Funding

This work was supported by the National Key Research and Development Program of China (2022YFD1201600); the National Natural Science Foundation of China (32373106, 31872556, and 31861123001); and the Chongqing Fishery Technology Innovation Union (CQFTIU2024-08).

Conflict of interest statement.

The authors declare that they have no known competing financial interests or personal relationships that could have appeared to influence the work reported in this paper.

Author contributions

Jia Xu (Data curation, Formal analysis, Investigation, Methodology, Writing – original draft), Peng Li (Methodology, Validation), Mengmeng Xu (Data curation, Methodology), Chenxu Wang (Supervision, Writing – review & editing), Tom Kocher (Writing – review & editing), and Deshou Wang (Supervision, Validation, Writing – review & editing)

Data availability

All the statistical data can be found on the *Journal of Heredity* online and the transcriptome data presented in this study are deposited in NCBI open database with the accession number PRJNA1102913.

References

Alonzo JR, Venkataraman C, Field MS, Stover PJ. The mitochondrial inner membrane protein MPV17 prevents uracil accumulation in mitochondrial DNA. J Biol Chem. 2018:293:20285–20294.

Antonenkov VD, Isomursu A, Mennerich D, Vapola MH, Weiher H, Kietzmann T, Hiltunen JK. The human mitochondrial DNA depletion syndrome gene *MPV17* encodes a non-selective channel that modulates membrane potential. J Biol Chem. 2015:290:13840–13861.

Artuso L, Romano A, Verri T, Domenichini A, Argenton F, Santorelli FM, Petruzzella V. Mitochondrial DNA metabolism in early development of zebrafish (*Danio rerio*). Biochim Biophys Acta. 2012:1817:1002–1011.

Basel D. Mitochondrial DNA depletion syndromes. Clin Perinatol. 2020:47:123–141.

Bian WP, Pu SY, Xie SL, Wang C, Deng S, Strauss PR, Pei DS. Loss of *mpv17* affected early embryonic development via mitochondria dysfunction in zebrafish. Cell Death Discov. 2021:7:250.

Boore JL. Animal mitochondrial genomes. Nucleic Acids Res. 1999:27:1767–1780.

Bratic I, Trifunovic A. Mitochondrial energy metabolism and ageing. Biochim Biophys Acta. 2010:1797:961–967.

Curran K, Lister JA, Kunkel GR, Prendergast A, Parich M, Raibl DW. Interplay between Foxd3 and Mitf regulates cell fate plasticity in the zebrafish neural crest. Dev Biol. 2010:344:107–118.

D'Agati G, Beltre R, Sessa A, Burger A, Zhou Y, Mosimann C, White RM. A defect in the mitochondrial protein Mpv17 underlies the transparent *casper* zebrafish. Dev Biol. 2017:430:11–17.

D'Mello SA, Finlay GJ, Baguley BC, Askarian-Amiri ME. Signaling pathways in melanogenesis. Int J Mol Sci. 2016:17:1144.

Dalla Rosa I, Cámara Y, Durigon R, Moss CF, Vidoni S, Akman G, Hunt L, Johnson MA, Grocott S, Wang L, et al. MPV17 loss causes deoxynucleotide insufficiency and slow DNA replication in mitochondria. PLoS Genet. 2016:12:e1005779.

Dallabona C, Marsano RM, Arzuffi P, Ghezzi D, Mancini P, Zeviani M, Ferrero I, Donnini C. Sym1, the yeast ortholog of the MPV17 human disease protein, is a stress-induced bioenergetic and morphogenetic mitochondrial modulator. Hum Mol Genet. 2010:19:1098–1107.

De Vitto H, Arachchige DB, Richardson BC, French JB. The intersection of purine and mitochondrial metabolism in cancer. Cells. 2021:10:2603.

Denton EJ, Land MF. Mechanism of reflexion in silvery layers of fish and cephalopods. Proc R Soc Lond B Biol Sci. 1971:178:43–61.

Dutton KA, Pauliny A, Lopes SS, Elworthy S, Carney TJ, Rauch J, Geisler R, Haffter P, Kelsh RN. Zebrafish *colourless* encodes *sox10* and specifies non-ectomesenchymal neural crest fates. Development. 2001:128:4113–4125.

El-Hattab AW, Craigen WJ, Scaglia F. Mitochondrial DNA maintenance defects. Biochim Biophys Acta Mol Basis Dis. 2017:1863:1539–1555.

El-Hattab AW, Li FY, Schmitt E, Zhang S, Craigen WJ, Wong LJ. MPV17-associated hepatocerebral mitochondrial DNA depletion syndrome: new patients and novel mutations. Mol Genet Metab. 2010:99:300–308.

El-Hattab AW, Scaglia F. Mitochondrial cytopathies. Cell Calcium. 2016:60:199–206.

Fenech M. The role of folic acid and Vitamin B12 in genomic stability of human cells. Mutat Res. 2001:475:57–67.

Field MS, Kamynina E, Chon J, Stover PJ. Nuclear folate metabolism. Annu Rev Nutr. 2018:38:219–243.

Fox JT, Stover PJ. Folate-mediated one-carbon metabolism. Vitam Horm. 2008:79:1–44.

French JB, Jones SA, Deng H, Pedley AM, Kim D, Chan CY, Hu H, Pugh RJ, Zhao H, Zhang Y, et al. Spatial colocalization and functional link of purinosomes with mitochondria. Science. 2016:351:733–737.

Frohnhöfer HG, Krauss J, Maischein HM, Nüsslein-Volhard C. Iridophores and their interactions with other chromatophores are required for stripe formation in zebrafish. Development. 2013:140:2997–3007.

Fujii R. The regulation of motile activity in fish chromatophores. Pigment Cell Res. 2000:13:300–319.

Giles RE, Blanc H, Cann HM, Wallace DC. Maternal inheritance of human mitochondrial DNA. Proc Natl Acad Sci U S A. 1980:77:6715–6719.

González-Vioque E, Torres-Torronteras J, Andreu AL, Martí R. Limited dCTP availability accounts for mitochondrial DNA depletion in mitochondrial neurogastrointestinal encephalomyopathy (MNGIE). PLoS Genet. 2011:7:e1002035.

Gur D, Bain EJ, Johnson KR, Aman AJ, Pasolli HA, Flynn JD, Allen MC, Deheyn DD, Lee JC, Lippincott-Schwartz J, et al. In situ differentiation of iridophore crystallotypes underlies zebrafish stripe patterning. Nat Commun. 2020:11:6391.

Karadimas CL, Vu TH, Holve SA, Chronopoulou P, Quinzii C, Johnsen SD, Kurth J, Eggers E, Palenzuela L, Tanji K, et al. Navajo neurohepatopathy is caused by a mutation in the MPV17 gene. Am J Hum Genet. 2006:79:544–548.

Kelsh RN, Harris ML, Colanesi S, Erickson CA. Stripes and belly-spots—a review of pigment cell morphogenesis in vertebrates. Semin Cell Dev Biol. 2009:20:90–104.

Kim D, Paggi JM, Park C, Bennett C, Salzberg SL. Graph-based genome alignment and genotyping with HISAT2 and HISAT-genotype. Nat Biotechnol. 2019:37:907–915.

Kimura T, Takehana Y, Naruse K. *pnp4a* is the causal gene of the medaka iridophore mutant *guanineless*. G3 (Bethesda). 2017:7:1357–1363.

Kottler VA, Künstner A, Koch I, Flötenmeyer M, Langenecker T, Hoffmann M, Sharma E, Weigel D, Dreyer C. Adenylate cyclase 5 is required for melanophore and male pattern development in the guppy (*Poecilia reticulata*). Pigment Cell Melanoma Res. 2015:28:545–558.

Krauss J, Astrinidis P, Frohnhöfer HG, Walderich B, Nüsslein-Volhard C. Erratum: *transparent*, a gene affecting stripe formation in Zebrafish, encodes the mitochondrial protein Mpv17 that is required for iridophore survival. Biol Open. 2013:2:979.

Lang MR, Patterson LB, Gordon TN, Johnson SL, Parichy DM. Basonuclin-2 requirements for zebrafish adult pigment pattern development and female fertility. PLoS Genet. 2009:5:e1000744.

Le Douarin NM, Dupin E. Multipotentiality of the neural crest. Curr Opin Genet Dev. 2003:13:529–536.

Lee D, Xu IM, Chiu DK, Lai RK, Tse AP, Lan Li L, Law CT, Tsang FH, Wei LL, Chan CY, et al. Folate cycle enzyme MTHFD1L confers metabolic advantages in hepatocellular carcinoma. J Clin Invest. 2017:127:1856–1872.

Li M, Yang H, Zhao J, Fang L, Shi H, Li M, Sun Y, Zhang X, Jiang D, Zhou L, et al. Efficient and heritable gene targeting in tilapia by CRISPR/Cas9. Genetics. 2014:197:591–599.

Löllgen S, Weiher H. The role of the Mpv17 protein mutations of which cause mitochondrial DNA depletion syndrome (MDDS): lessons from homologs in different species. Biol Chem. 2015:396:13–25.

López LC, Akman HO, García-Cazorla A, Dorado B, Martí R, Nishino I, Tadesse S, Pizzorno G, Shungu D, Bonilla E, et al. Unbalanced deoxynucleotide pools cause mitochondrial DNA instability in thymidine phosphorylase-deficient mice. Hum Mol Genet. 2009:18:714–722.

Lu B, Wang C, Liang G, Xu M, Kocher TD, Sun L, Wang D. Generation of ornamental *Nile tilapia* with distinct gray and black body color pattern by *csf1ra* mutation. Aquacult Rep. 2022:23:101077.

Martorano L, Peron M, Laquatra C, Lidron E, Facchinello N, Meneghetti G, Tiso N, Rasola A, Ghezzi D, Argenton F. The zebrafish orthologue of the human hepatocerebral disease gene *MPV17* plays pleiotropic roles in mitochondria. Dis Model Mech. 2019:12:dmm037226.

Moss CF, Dalla Rosa I, Hunt LE, Yasukawa T, Young R, Jones AWE, Reddy K, Desai R, Virtue S, Elgar G, et al. Aberrant ribonucleotide incorporation and multiple deletions in mitochondrial DNA of the murine MPV17 disease model. Nucleic Acids Res. 2017:45:12808–12815.

Mukherje S, Das S, Bedi M, Vadupu L, Ball WB, Ghosh A. Methylglyoxal-mediated Gpd1 activation restores the mitochondrial defects in a yeast model of mitochondrial DNA depletion syndrome. Biochim Biophys Acta Gen Subj. 2023:1867:130328.

Ng A, Uribe RA, Yieh L, Nuckels R, Gross JM. Zebrafish mutations in *gart* and *paics* identify crucial roles for de novo purine synthesis in vertebrate pigmentation and ocular development. Development. 2009:136:2601–2611.

Parichy DM, Mellgren EM, Rawls JF, Lopes SS, Kelsh RN, Johnson SL. Mutational analysis of *endothelin receptor b1* (*rose*) during neural crest and pigment pattern development in the zebrafish *Danio rerio*. Dev Biol. 2000:227:294–306.

Patterson LB, Parichy DM. Interactions with iridophores and the tissue environment required for patterning melanophores and xanthophores during zebrafish adult pigment stripe formation. PLoS Genet. 2013:9:e1003561.

Petratou K, Spencer SA, Kelsh RN, Lister JA. The MITF paralog *tfec* is required in neural crest development for fate specification of the iridophore lineage from a multipotent pigment cell progenitor. PLoS One. 2021:16:e0244794.

Petratou K, Subkhankulova T, Lister JA, Rocco A, Schwetlick H, Kelsh RN. A systems biology approach uncovers the core gene regulatory network governing iridophore fate choice from the neural crest. PLoS Genet. 2018:14:e1007402.

Schartl M, Larue L, Goda M, Bosenberg MW, Hashimoto H, Kelsh RN. What is a vertebrate pigment cell? Pigment Cell Melanoma Res. 2016:29:8–14.

Spinazzola A. Mitochondrial DNA mutations and depletion in pediatric medicine. Semin Fetal Neonatal Med. 2011:16:190–196.

Spinazzola A, Viscomi C, Fernandez-Vizarra E, Carrara F, D'Adamo P, Calvo S, Marsano RM, Donnini C, Weiher H, Strisciuglio P, et al. MPV17 encodes an inner mitochondrial membrane protein and is mutated in infantile hepatic mitochondrial DNA depletion. Nat Genet. 2006:38:570–575.

Steele JW, Kim SE, Finnell RH. One-carbon metabolism and folate transporter genes: do they factor prominently in the genetic etiology of neural tube defects? Biochimie. 2020:173:27–32.

Suomalainen A, Isohanni P. Mitochondrial DNA depletion syndromes—many genes, common mechanisms. Neuromuscul Disord. 2010:20:429–437.

Wang C, Lu B, Li T, Liang G, Xu M, Liu X, Tao W, Zhou L, Kocher TD, Wang D. Nile Tilapia: a model for studying teleost color patterns. J Hered. 2021:112:469–484.

Wasmeier C, Hume AN, Bolasco G, Seabra MC. Melanosomes at a glance. J Cell Sci. 2008:121:3995–3999.

Weiher H, Noda T, Gray DA, Sharpe AH, Jaenisch R. Transgenic mouse model of kidney disease: insertional inactivation of ubiquitously expressed gene leads to nephrotic syndrome. Cell. 1990:62:425–434.

Zhang L, Wan M, Tohti R, Jin D, Zhong TP. Requirement of zebrafish *adcy3a* and *adcy5* in melanosome dispersion and melanocyte stripe formation. Int J Mol Sci. 2022a:23:14182.

Zhang W, Wang H, Brandt DYC, Hu B, Sheng J, Wang M, Luo H, Li Y, Guo S, Sheng B, et al. The genetic architecture of phenotypic diversity in the Betta fish *(Betta splendens*). Sci Adv. 2022b:8:eabm4955.

Zhou X, Solaroli N, Bjerke M, Stewart JB, Rozell B, Johansson M, Karlsson A. Progressive loss of mitochondrial DNA in thymidine kinase 2-deficient mice. Hum Mol Genet. 2008:17:2329–2335.